Fast and Green Hematite (α-Fe₂O₃) and Akaganeite (β-FeOOH) Synthesis Using a Microwave-Assisted Hydrothermal Process with Single Precursor and No Stabilizing Agent

Paulo Afonso F. Diniz[a], Kiany Sirley B. Cavalcante[a], Josiane Carneiro Souza[b],

Gleison N. Marques[b], Fernanda Hellen de S. Santos[c] , Fiama M. Cutrim[b],

Raelma B. Henriques[d], Leonardo T. B. Mendonça[e*] , Ulisses M. Nascimento[f]

[a]*Instituto Federal do Maranhão, Programa de Pós-Graduação em Química, São Luís, MA, Brasil.*
[b]*Instituto de pesquisa científica em São Carlos, Centro de Desenvolvimento de Materiais Funcionais, São Carlos, SP, Brasil.*
[c]*Universidade Federal do Maranhão, Núcleo de Análise de Resíduos Pesticidas, São Luís, MA, Brasil.*
[d]*Universidade Federal do Maranhão, Núcleo de Combustíveis Catálise e Ambiental, São Luís, MA, Brasil.*
[e]*Universidade Federal do Maranhão, São Luís, MA, Brasil.*
[f]*Universidade Federal do Maranhão, Programa de Pós-Graduação em Energia e Ambiente, São Luís, MA, Brasil.*

In this work, iron chloride (FeCl₃.6H₂O), a single reagent, was used to create the phases of hematite (α-Fe₂O₃) and akaganeite (β-FeOOH) without the need of organic solvents using the microwave-assisted hydrothermal technique (HM). X-ray diffraction demonstrated the efficacy of the HM technique in the generation of crystalline phases of α-Fe₂O₃ at 180°C and β-FeOOH at 120°C. The development of pseudo-cunic and stick-like particles was a result of changes in experimental variables, which also had a substantial impact on the materials structural characteristics. The nitrogen (N₂) adsorption/desorption isotherms of the samples containing akaganeite and hematite phase resembled those of mesoporous materials. Hematite has a surface area of 25.44 m² g⁻¹, while akaganeite has a surface area of 110.60 m² g⁻¹, according to the calculation. Thermodifferential and thermogravimetric techniques were used to assess thermal degradation. The use of microwave hydrothermal synthesis was promoted as being quick, easy, affordable, and safe for the environment.

Keywords: *Hematite, Akaganeite, fast synthesis, green metfhod, high surface área.*

1. Introduction

In the literature, there has been an increase in interest in the search for ecologically friendly synthesis methods[1-3]. Green chemistry and its 12 principles seek to ensure a process with a low level of waste generation in accordance with the principles that guide conscientious and sustainable behavior[4]. The biggest obstacle in developing synthetic methods that adhere to these principles is the complete or partial replacement of ecologically hazardous solvents with those that provide little to no risk[5].

Thus, the usage of fuels, organic solvents, and surfactants as a way of enhancing the process of producing such materials is frequently observed in the methods of synthesis of ceramic compounds, such as sol-gel, combustion, co-precipitation, and hydrothermal[6-9]. The selection of the synthesis method and the related chemicals becomes even more crucial when the application to which this material will be submitted and the anticipated features, such as particle size and shape, are taken into account[10,11].

A case in point of a material whose morphological and structural features can be changed depending on the treatment is hematite (α-Fe₂O₃) and akaganite (β-FeOOH). Both phases, which are produced by the F-O-H system, have a wide range of potential applications as well as outstanding stability and minimal toxicity[12,13]. In a recent study, Kushwaha and Chauhan[14] synthesized α-Fe₂O₃ via the co-precipitation method. They used the surfactant ethylenediaminetetraacetic acid (EDTA) to simulate the size and form of the particles[14]. Norouzi and Nezamzadeh-Ejhieh[15] synthesized α-Fe₂O₃ using silver nitrate (AgNO₃) and ethanol, followed by pH adjustment, to create a heterostructure of α-Fe₂O₃/Cu₂O for the photodegradation of the methylene blue dye[15].

In order to produce α/β-FeOOH for testing in oxygen evolution reactions (OER)[16] used a solvothermic route modified with different concentrations of iron chloride (FeCl₃), sodium nitrate (NaNO₃), hydrochloric acid (HCl), acetonitrile (CH₃CN) and sodium hydroxide (NaOH). Through this study, it was found that the metallic precursor and the solvent used are fundamental for the formation of FeOOH phases. Despite this, there are few works that present the

synthesis of hematite and akaganeite from a single precursor and, even so, they used conventional hydrothermal method with long reaction period and high energy consumption with no selective production of the compounds[17-19].

In this study, α-Fe$_2$O$_3$ and β-FeOOH were prepared using the microwave-assisted hydrothermal method (HM) and without use of organic solvents in the one fast step. Changes in the morphology of materials were investigated from experimental conditions such as time and concentration of the precursor.

2. Experimental Procedure

2.1. Synthesis of the β-FeOOH and α-Fe$_2$O$_3$ powders

Iron chloride hexahydrate (FeCl$_3$.6H$_2$O, P.A., Synth) was used in a microwave-assisted hydrothermal synthesis. In the Teflon reaction cell, 100 mL of the FeCl$_3$.6H$_2$O aqueous solution with a concentration of 0.1, 0.3 and 0.5 mol L^{-1} with different conditions of time and temperature was used (Table 1). Then, the cell was sealed and taken to an adapted domestic microwave hydrothermal system, operating at 2.45 GHz and maximum power of 800 W. After the reaction time, the final product was centrifuged at 4000 rpm for 30 minutes and washed with distilled water 5 times. After that, the material was dried at 60 ºC for 12 hours in an oven.

2.2. Characterization techniques

The thermogravimetric (TGA) and thermodifferential (DTG) analyzes of the materials produced were performed in a Netzsch – 409 Cell equipment, using alumina as a reference material, heated up to 1000 °C in an oxygen atmosphere with a flow of 50 mL min^{-1} and heating rate of 10 °C min^{-1}. The crystal structure was analyzed by X-Ray Diffraction (XRD) in a Bruker Diffractometer (D8 Advanced), using CuKα radiation (λ= 1.5406 Å), operating in the angular range of 20° to 70° with a step of 0.02 ° and counting time of 2s. The indexed phases were refined using the Rietveld method[20] using the Maud program version 2.33[21,22]. The average crystallite size of each sample was calculated using the Scherrer formula expressed in Equation 1.

$$D = \frac{k\lambda}{\beta Cos\theta} \tag{1}$$

where K refers to the form factor (0.9), λ is the wavelength of Cu Kα=0.15418 nm, β is o the full width at half maximum (FWHM in radians) and the diffraction angle θ. In each sample, the peak with intensity of 100% was chosen for the calculation of crystallite size.

The morphology of the particles was investigated by Scanning Field Emission Electron Microscopy (SEM-FEG), PHILIPS XL, using a secondary electron detector with an incident beam of 25 vK. The specific surface area measurements of the samples were determined by the Branauer-Emmett-Teller (BET) method, using a Quantacrome analyzer.

3. Results and Discussion

3.1. X-ray diffraction (XRD) and Rietveld Refinement

Figure 1 shows the X-ray diffractograms of samples β-1, β-2, and β-3. As can be seen in Figure 1D, all samples exhibit diffraction peaks associated with the single phase

Table 1. Experimental conditions used in synthesis of β-FeOOH and α-Fe$_2$O$_3$.

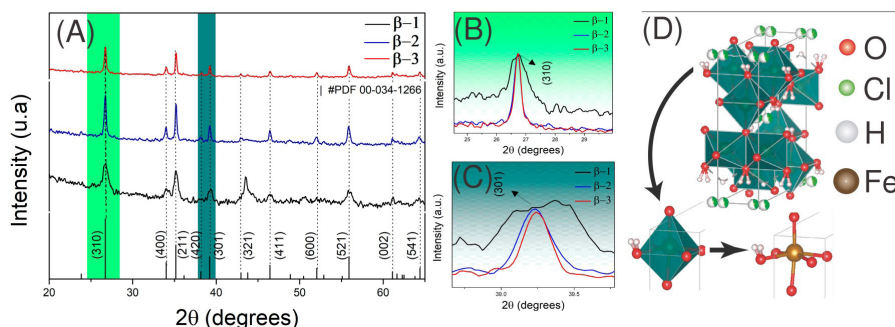| Samples	Subtitle	Parameters		
		Concentration (mol. L^{-1})	Time (min)	Temperature (°C)
Akaganeite	β-1	0.1	4	120
Akaganeite	β-2	0.5	4	120
Akaganeite	β-3	0.3	8	150
Hematite	α-1	0.1	4	180
Hematite	α-2	0.5	4	180

Figure 1. (A) X-ray diffractograms of samples β-1, β-2 and β-3 (B) magnification of the highest intensity peak region (310), (C) magnification of the peak region (301) and (D) graphic representation of the octahedral clusters forming the unit cell of the Akaganeite phase.

Fast and Green Hematite (α-Fe₂O₃) and Akaganeite (β-FeOOH) Synthesis Using a Microwave-Assisted
Hydrothermal Process with Single Precursor and No Stabilizing Agent

3

β-FeOOH (PDF 34-1266), which has a tetragonal structure. It is feasible to confirm the narrowing of the diffraction peaks by analyzing the diffractograms of the β-2 and β-3 samples; this phenomena is best seen in Figure 1B-1C, with approximation of the planes (310) and (301), respectively, and denotes an increase in phase crystallinity[23], which is expected when the microwave-assisted hydrothermal method is applied, which has the advantage of direct crystallization of the desired phase[24] in a time less than 10 min as observed in samples β-2 and β-3 with 4 and 8 minutes respectively.

The synthesis of zinc tungstate ($ZnWO_4$) generated with and without microwave-assisted hydrothermal treatment was compared by Andrade et al.[25] in 2020. The samples that were obtained following irradiation displayed more crystallinity, according to the authors. Additionally, the duration of the heat treatment was also taken into account by the authors, and longer heat treatment times resulted in more intense peaks being seen in the samples[25].

The concentration of the metallic precursor must also be taken into account as a significant factor to explain the narrowing of the samples' diffraction peaks. As was shown at constant temperature and time, higher concentrations cause the diffraction lines to narrow, as was seen in the sample β-2. (0.5 mol L^{-1}), on the other hand, at a lower concentration of precursor, this narrowing does not occur in a marked way, as demonstrated in sample β-1 (0.1 mol L^{-1}). As seen in the β-3 sample, it is possible to create a sample with good crystallinity even at low concentrations, assuming that the synthesis parameters, time, and temperature are altered.

The diffractograms of the α-1 and α-2 samples in Figure 2 show the diffraction peaks for the hematite phase (α-Fe_2O_3), which is characterized by the rhombohedral crystal system and R-3c space groups (Figure 1C) (A). (PDF 33-0664).

The absence of secondary phase peaks in the diffractograms is evidence of the success of the HM process in generating pure α-Fe_2O_3. The samples displayed high crystallinity, however as seen in Figure 2B, the α-2 sample had narrower peaks than the α-1 sample, with amplification of the peaks of maximum intensity (104) and (110). Furthermore, there isn't much of a displacement between the peaks. The time and temperature adopted in the synthesis of powders are lower than those found in the literature for the conventional hydrothermal method[26-28].

Since the Fe^{3+} ions are wrapped in a hydration sphere—that is, water molecules couple around these ions due to the predominantly high dielectric constant of water (78.8 at 25 °C)—and electromagnetic radiation causes the oscillatory motion of water molecules, this behavior of shortening the time to obtain the α-Fe_2O_3 phase may be related to the use of microwave energy[29]. Cai et al.[29] observed similar outcomes for the decrease of synthesis time utilizing microwave heating.

Using the Debye-Scherrer equation and the half-height width (FWHM) of the diffraction peaks with the highest intensities of the β-FeOOH (310) and α-Fe_2O_3 (104) phases as data, the crystallite sizes of the samples were calculated. This indicates that when the FWHM drops, the diffraction peaks become narrower and the crystallite size increases[30], as seen in samples β-2 and β-3, which displayed smaller FWHM values of 0.19 and 0.20, respectively, and bigger crystallite sizes of 43.60 and 42.05, respectively. In every sample that was synthesized, this behavior was seen.

By using the Rietveld method to refine crystal structures from X-ray diffraction data, it is possible to obtain information about the structural and chemical content of the generated phases[31]. Although the samples were subjected to various experimental settings, it can be seen from the sample refinement data in Table 2 that neither the network parameters nor the
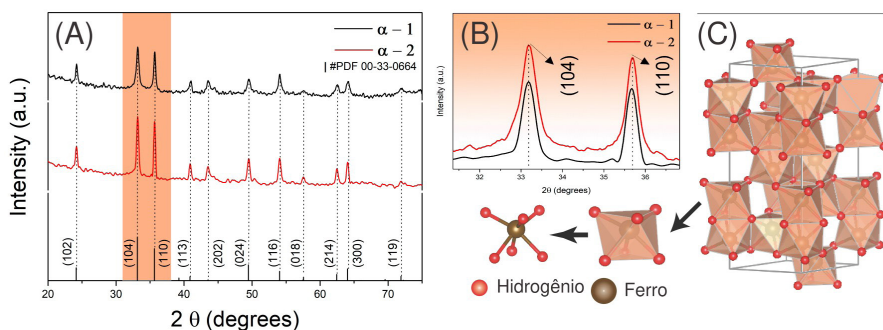

Figure 2. (A) X-ray diffractograms of the samples α-1 and α-2 (B) magnification of the region of the highest intensity peaks (104) and (110), (C) graphic representation of the octahedral clusters forming the unit cell of the hematite phase.

Table 2. Crystallographic and statistical parameter values obtained through Rietveld refinement.

| | Crystallographic parameters | | | | | χ^2 | RWp |
	a (Å)	b (Å)	c (Å)	V (Å)	β		
β-1	10.55	10.55	3.03	337.24	89.15	1.13	4.03
β-2	10.58	10.58	3.03	339.16	90,195	1.14	4.21
β-3	10.56	10.56	3.03	337.86	89,895	1.14	4.18
α-1	5.04	13.78	5.04	350.03	***	1.28	4.53
α-2	5.04	13.78	5.04	350.03	***	1.26	4.40

χ^2 = fit quality, Rwp = profile fit, β = axial angle, a, b, c = lattice parameters. ***No values.

unit cell volume significantly changed between the β-1, β-2 and β-3 phases or between the α-1 and α-2 samples. The hematite samples' different precursor concentrations had no noticeable impact on the network parameters, as both samples displayed the same values a=5.04 and c=13.78. The degree of refinement and fit of the predicted diffractogram to the observed diffractogram are represented, respectively, by the statistical parameters of χ^2 and RWp. The results for all synthetic samples showed χ^2 and RWp values below 1.5 and 5, respectively, demonstrating the effectiveness of the sample treatment[31].

3.2. Thermal analysis

Figure 3 displays the thermodifferential (DTA) and thermogravimetric (TG) curves of the powders created. The TG curves of samples β-1 and β-3 in Figure 3A and 3C can be used to demonstrate the stability of mass loss, while sample β-2 in Figure 3B only exhibits a comparable behavior after 600°C due to the high precursor concentration that causes more Cl⁻ in the sample to be volatilized. Similar phenomenon was reported by Fu et al.[32], who explained it by the elimination of water and chloride ions, followed by the structural change from the tetragonal β-FeOOH phase to the rhombohedral α-Fe₂O₃ phase[32]. A peak of the DTA curve that is exodothermic (Figure 3A) at 360 °C may be related to the dehydroxylation and volatilization of hydroxyl and chloride ions in the β-1 sample, which showed a mass loss of about 21%[33,34]. The concentration of the precursor used in the β-2 and β-3 samples and the elimination process of OH- and Cl- provide the main explanations for the endothermic peaks seen in the samples at regions close to temperatures of 610 and 520 °C, respectively[34,35].

Chloride ions maintain the stability of the β-FeOOH phase, and when they are removed during the heat treatment process, either in structural tunnels or on the particle surface, akaganeite changes into hematite[29,33]. While sample β-1 exhibits a mass loss of about 300 °C and a continual

escape of Cl⁻ that is likely the result of deeper structural tunnels, sample β-3 exhibits an abrupt mass loss of about 350 °C and a primary loss of the chloride ion from the surface of the particles[33].

The α-1 and α-2 samples (Figure 3D-3E) show greater stability, with mass loss of 3.5% and 6.5%, respectively. The thermodifferential curve of the α-1 sample showed an endothermic peak between ≈ 385 ºC and ≈ 490 ºC and the α-2 sample at ≈ 400 ºC, both characteristic of the elimination of chloride ions from the precursor of the synthesis[36], and an exothermic peak at ≈ 534 °C attributed to recrystallization of hematite[37]. Furthermore, in the DTA curves of α-1 and α-2, there are endothermic peaks at approximately 110 ºC that are characteristic of the loss of hydration water in the studied samples[36,38].

3.3. Morphological analysis

Figure 4 displays the morphologies of the particles of β-FeOOH and α-Fe₂O₃. The samples β-1, β-2 and β-3 (Figure 4B-4C) display significantly agglomerated particles, while sample 1 (Figure 4A) had a non-equiaxial shape. Figure 4G, which shows nanorod-shaped particles with an average length of 170 nm that are securely connected to the surfaces of bigger particles, provides a clear illustration of this fact. This average size is smaller than that reported by Yang et al.[39], who used the traditional hydrothermal method to synthesize nanorods β-FeOOH with an average size of 191 nm over reaction times of 3 to 48 hours[39]. The particles created by Li et al.[40], to anchor them under a superhydrophobic Polyvinylidene Fluoride (PVDF) membrane, displayed the same form[40].

The quantity of nanorods on the surface of the bigger particles accounts for the majority of the variation shown in the micrographs of samples β-1 to β-3 (Figure 4A-4C). Changes in the quantities of iron chloride present and the heat treatment temperatures applied throughout the synthesis largely account for this phenomenon. Although Cho et al.[41] used the
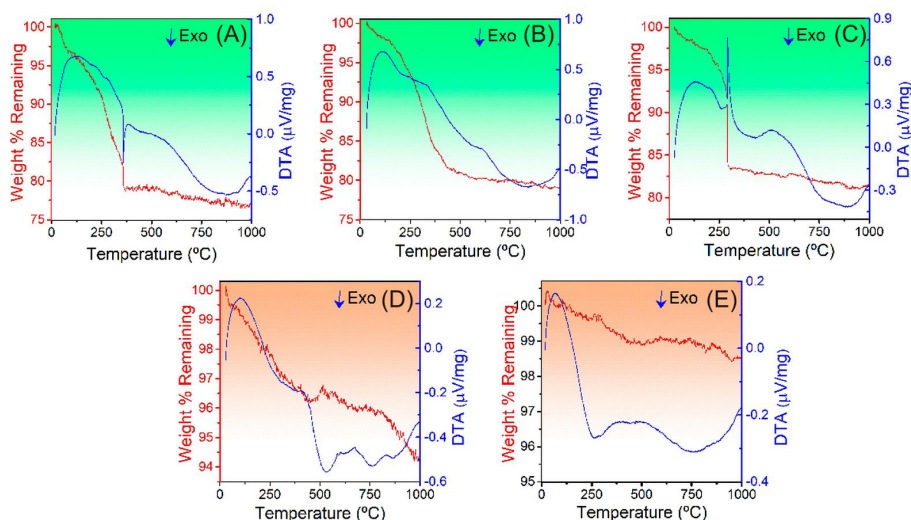

Figure 3. Thermogravimetric and thermodifferential curves of the samples: (A) β-1, (B) β-2, (C) β-3, (D) α-1 and (E) α-2 heated up to 1000 ºC in a flow of 50 mL min⁻¹ of O₂.

precipitation strategy and needed more than 8 days for the synthesis, they also reported the production of nanorods[41]. The samples α-1 and α-2 particles, which have a spherical shape and a size distribution between 500 and 600 nm, can be seen in the micrographs of Figure 4D-4F. These particles with controlled shape and narrow size distribution were quickly achieved without the use of organic solvents like sodium carboxymethyl cellulose (CMC), which slows the growth particles[10]. When HM synthesis is contrasted to other methods of generating akaganeite and hematite, different particle sizes and shapes are observed. For instance, Tang et al.[42] produced arrays of β-FeOOH nanorods with a mean diameter ranging from 50 to 100 nm using the hydrothermal method[42]. Li et al.[43] created nanorods that ranged in size from 90 to 200 nm and demonstrated that the morphological properties might change depending on the hydrothermal synthesis settings[43].

3.4 Surface area analysis

The nitrogen (N_2) adsorption/desorption isotherms are shown in Figure 5. The akaganeite samples type IV isotherms are typical of materials with robust solid/gas interactions. This type of action is typically seen in mesoporous materials[44]. In the β-1 sample, the H2-type hysteresis loop demonstrated mesoporosity with a variety of effects on the pore network. At a P/P° of 0.42, the desorption branch of this sample underwent hysteresis closure, indicating the presence of two different kinds of mesopores. The 4 nm pores are shown by the lower closure value[45].

Furthermore, as can be seen in Table 3, sample β-1 had the largest specific area, 100.60 $m^2 g^{-1}$. The variation in pore diameter of samples β-1 to β-3 remained within the range between 12.08 and 29.36 nm respectively.

The hematite samples (Figure 5D-5E) did not exhibit such a marked change in these pore diameter values with regard to
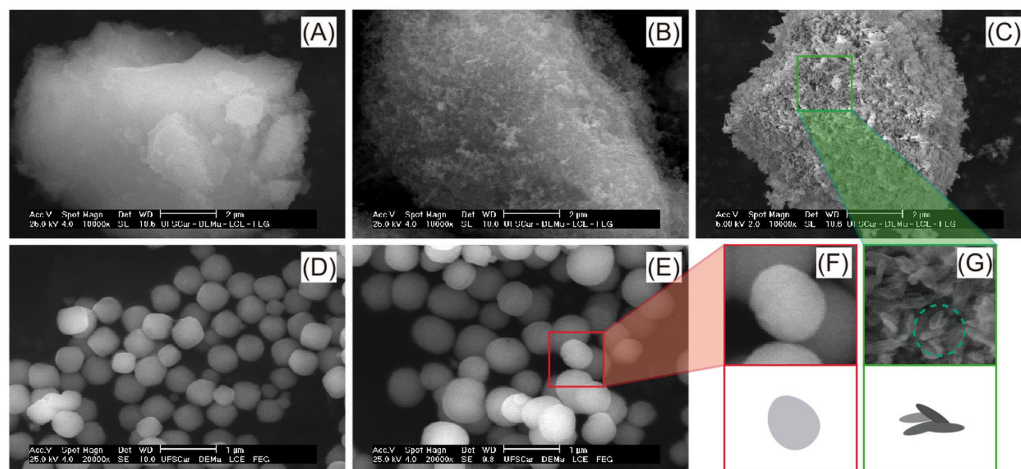

Figure 4. Micrographs of samples (A) β-1, (B) β-2, (C) β-3, (D) α-1 and (E) α-2, (F) schematic representation of the shape of hematite particles and (G) schematic representation of the shape of Akaganeite particles.
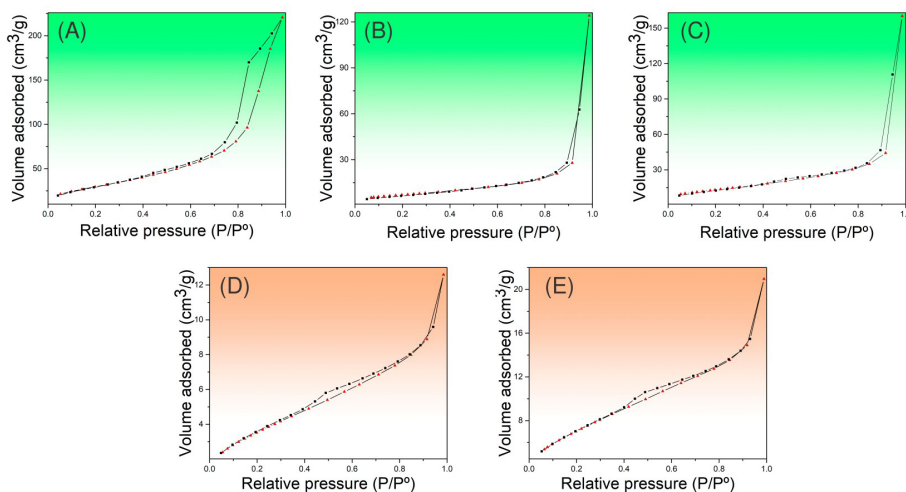

Figure 5. Adsorption/Desorption isotherms for akaganeite (β-FeOOH) and hematite (α-Fe₂O₃).

Table 3. Surface properties for akaganeite (β-FeOOH) and hematite (α-Fe$_2$O$_3$).

Samples	surface area (m^2 g^{-1})	Average size of the pores (nm)
β-1	100.60	12.08
β-2	26.15	29.36
β-3	48.84	20.28
α-1	13.43	5.80
α-2	25.44	5.10

Table 4. Comparison of conditions for synthesis of hematite and akageneite in currently published works

REF.	Synthesis Method	time reaction	phase crystalline	morphology	surface area	capping agent
[48]	Hydrothermal conventional	48 hours	akaganeite	nanorods	-	-
[49]	Controlled Preciptation	1/192 hours	akaganeite/ hematite	nanorods/ microcubes	-	-
[50]	Hydrothermal conventional	6 hours	akaganeite	elipsoids/ nanoneedles	-	3,3-thiodipropionic acid
[51]	Controlled preciptation	1 hour	akaganeite	nanorods	120 m^2.g^{-1}	vegetal extract
This work	Microwave assited hydrothermal	8 min	akaganeite/ hematite	nanorods/ nanospheres	100.6/25.4 m^2/g^{-1}	-

pore size (5.80 and 5.10 nm). The isotherms for adsorption and desorption are of type IV[46]. The surface properties information in these samples did not vary significantly, but the sample 1 specific area (25.44 m^2 g^{-1}) is higher than the sample 2 specific area (13.43 m^2 g^{-1}) in value, Kim et al.[10] and Katsuki et al.[47] synthesized hematite, by a simple hydrothermal system, and obtained a specific area ranging from 6.63 to 7.90 m^2 g^{-1} and from 2.26 to 5.01 m^2 g^{-1}, thus demonstrating the effectiveness of HM synthesis for the production of hematite with elevated surface area[10,47]. Table 4 shows a comparison between different synthesis methods and information on morphology and surface area demonstrating that this work has the advantage of fast synthesis time associated with a high surface area to akaganeite/hematite.

4. Conclusion

The hydrothermal method assisted with microwave irradiation proved to be efficient to obtain iron oxide in the hematite phase and hydroxide oxide in the akaganeite phase. Changes in experimental conditions such as concentration of the metallic precursor, time and temperature of synthesis were fundamental for the phase change. Temperature was the determining parameter for obtaining different phases, in which the temperature of 180 °C favored the formation of α-Fe$_2$O$_3$, and below this temperature, there is a favoring of β-FeOOH formation. In the morphological characteristics of both phases, the variation in the range of synthesis parameters led to changes in particle morphology, crystallinity and surface area. Although the β-1 sample (0.1 mol L^{-1}, 4 min and 120 °C) has lower crystallinity than the other akaganeite samples, it had a larger specific area (100.60 m^2 g^{-1}). For the α-Fe$_2$O$_3$ samples, the main change caused by the change in the synthesis variables was in the specific area, as the α-2 sample had almost twice the surface area compared to the α-1 sample.

The applied methodology proved to be simpler, faster, more economical and efficient in the synthesis of ceramic compounds with a route that fits in several principles of Green Chemistry (safe chemistry, non-toxic products, energy saving, not using additional products or additives, accident prevention, atomic economics), in addition to proposing a synthesis using only one reagent as a precursor, a result that is little presented in the literature.

5. Acknowledgements

6. References

1. Mahmoud ME, Amira MF, Abouelanwar ME, Salam MA. Green synthesis and surface decoration of silver nanoparticles onto δ-FeOOH-Polymeric nanocomposite as efficient nanocatalyst for dyes degradation. J Environ Chem Eng. 2021;9(1):104697. http://dx.doi.org/10.1016/j.jece.2020.104697.

2. Kunoh T, Takeda M, Matsumoto S, Suzuki I, Takano M, Kunoh H et al. Green synthesis of gold nanoparticles coupled with nucleic acid oxidation. ACS Sustain Chem& Eng. 2018;6:364-73. http://dx.doi.org/10.1021/acssuschemeng.7b02610.

3. Nadagouda MN, Hoag G, Collins J, Varma RS. Green synthesis of Au nanostructures at room temperature using biodegradable plant surfactants. Cryst Growth Des. 2009;9:4979-83. http://dx.doi.org/10.1021/cg9007685.

4. Marco BA, Rechelo BS, Tótoli EG, Kogawa AC, Salgado HRN. Evolution of green chemistry and its multidimensional impacts: a review. Saudi Pharm J. 2019;27:1-8. http://dx.doi.org/10.1016/j.jsps.2018.07.011.

Fast and Green Hematite (α-Fe₂O₃) and Akaganeite (β-FeOOH) Synthesis Using a Microwave-Assisted
Hydrothermal Process with Single Precursor and No Stabilizing Agent

7

5. Lenoir D, Schramm K-W, Lalah JO. Green chemistry: some important forerunners and current issues. Sustain Chem Pharm. 2020;18:100313. http://dx.doi.org/10.1016/j.scp.2020.100313.

6. Peretyazhko TS, Fox A, Sutter B, Niles PB, Adams M, Morris RV et al. Synthesis of akaganeite in the presence of sulfate: implications for akaganeite formation in Yellowknife Bay, Gale Crater, Mars. Geochim Cosmochim Acta. 2016;188:284-96. http://dx.doi.org/10.1016/j.gca.2016.06.002.

7. Marques GN, Oliveira TP, Teixeira MM, Lot AV, Nascimento MF, Rangel JHG et al. Synthesis of yttrium aluminate doped with Cr³⁺ using MgF₂–Na₂B₄O₇ as mineralizers to obtain red pigments for ceramic tiles application. Ceram Int. 2020;46:27940-50. http://dx.doi.org/10.1016/j.ceramint.2020.07.287.

8. Tangwatanakul W, Sirisathitkul C, Limphirat W, Yimnirun R. Synchrotron X-ray absorption of iron oxide (Fe₂O₃) nanoparticles: effects of reagent concentration and sonication in co-precipitation synthesis. Zhongguo Wuli Xuekan. 2017;55:845-52. http://dx.doi.org/10.1016/j.cjph.2017.02.012.

9. Sato J, Kobayashi M, Kato H, Miyazaki T, Kakihana M. Hydrothermal synthesis of magnetite particles with uncommon crystal facets. J Asian Ceram Soc. 2014;2:258-62. http://dx.doi.org/10.1016/j.jascer.2014.05.008.

10. Kim CW, Kang MJ, Van TK, Kang YS. A selective morphosynthetic approach for single crystalline hematite through morphology evolution via microwave assisted hydrothermal synthesis. J Ind Eng Chem. 2017;53:341-7. http://dx.doi.org/10.1016/j.jiec.2017.05.005.

11. Ren G, Wang X, Zhang Z, Zhong B, Yang L, Xu D et al. Facile synthesis of maghemite nanoparticle from waste green vitriol as adsorbent for adsorption of arsenite. J Mol Liq. 2018;259:32-9. http://dx.doi.org/10.1016/j.molliq.2018.02.132.

12. Dubey M, Wadhwa S, Kumar R. Synthesis of hematite/alginate beads nanocomposite and its application in organic dye removal. Mater Today Proc. 2020;28:70-3. http://dx.doi.org/10.1016/j.matpr.2020.01.302.

13. Zhang Y, Dong K, Liu Z, Wang H, Ma S, Zhang A et al. Sulfurized hematite for photo-Fenton catalysis. Progr Nat Sci Mater Int. 2017;27:443-51. http://dx.doi.org/10.1016/j.pnsc.2017.08.006.

14. Kushwaha P., Chauhan P. Synthesis of spherical and Rod-Like EDTA assisted α-Fe₂O₃ nanoparticles via co-precipitation method. Mater Today Proc. 2021;44(2):3086-90.

15. Norouzi A., Nezamzadeh-Ejhieh A. α-Fe₂O₃/Cu₂O heterostructure: brief characterization and kinetic aspect of degradation of methylene blue. Physica B Condens. 2020;599:412422.

16. Hu J, Li S, Chu J, Niu S, Wang J, Du Y et al. Understanding the phase-induced electrocatalytic oxygen evolution reaction activity on FeOOH nanostructures. ACS Catal. 2019;9(12):10705-11. http://dx.doi.org/10.1021/acscatal.9b03876.

17. Dong Q, Wang D, Yao J, Kumada N, Kinomura N, Takei T et al. Synthesis of hematite particles with various shapes by a simple hydrothermal reaction. J Ceram Soc Jpn. 2009;117:245-8. http://dx.doi.org/10.2109/jcersj2.117.245.

18. Kandori K, Ishikawa T. Preparation and microstructural studies on hydrothermally prepared hematite. J Colloid Interface Sci. 2004;272:246-8. http://dx.doi.org/10.1016/j.jcis.2003.08.075.

19. Yang S, Xu Y, Sun Y, Zhang G, Gao D. Size-controlled synthesis, magnetic property, and photocatalytic property of uniform α-Fe₂O₃ nanoparticles via a facile additive-free hydrothermal route. CrystEngComm. 2012;14:7915-21. http://dx.doi.org/10.1039/c2ce25929j.

20. Rietveld HM. A profile refinement method for nuclear and magnetic structures. J Appl Cryst. 1969;2:65-71. http://dx.doi.org/10.1107/s0021889869006558.

21. Lutterotti L, Matthies S, Wenk HR, Schultz AS, Richardson JW. Combined texture and structure analysis of deformed limestone from time-of-flight neutron diffraction spectra. J Appl Phys. 1997;81:594-600. http://dx.doi.org/10.1063/1.364220.

22. Lutterotti L, Bortolotti M, Ischia G, Lonardelli I, Wenk HR. Rietveld texture analysis from diffraction images. Z Kristallogr. 2007;26(Suppl 1):125-30. http://dx.doi.org/10.1524/zksu.2007.2007.suppl_26.125.

23. Xu Z, Yu Y, Fang D, Xu J, Liang J, Zhou L. Microwave-ultrasound assisted synthesis of β-FeOOH and its catalytic property in a photo-Fenton-like process. Ultrason Sonochem. 2015;27:287-95. http://dx.doi.org/10.1016/j.ultsonch.2015.05.039.

24. Suchanek WL, Riman RE. Hydrothermal synthesis of advanced ceramic powders. Adv Sci Technol. 2006;45:184-93. http://dx.doi.org/10.4028/www.scientific.net/AST.45.184.

25. Andrade NF No, Nunes TBO, Li M, Longo E, Bomio MRD, Motta FV. Influence of microwave-assisted hydrothermal treatment time on the crystallinity, morphology and optical properties of ZnWO₄ nanoparticles: photocatalytic activity. Ceram Int. 2020;46:1766-74. http://dx.doi.org/10.1016/j.ceramint.2019.09.151.

26. Tadic M, Trpkov D, Kopanja L, Vojnovic S, Panjan M. Synthesis conditions, structure, particle shape analysis, cytotoxicity and magnetic properties. J Alloys Compd. 2019;792:599-609. http://dx.doi.org/10.1016/j.jallcom.2019.03.414.

27. Trpkov D, Kopanja L, Tadi M. Hydrothermal synthesis, morphology, magnetic properties and self-assembly of hierarchical α-Fe₂O₃ (hematite) mushroom-, cube- and sphere-like superstructures. Appl Surf Sci. 2018;457:427-38. http://dx.doi.org/10.1016/j.apsusc.2018.06.224.

28. Nassar MY, Ahmed IS, Hendy HS. A facile one-pot hydrothermal synthesis of hematite (α-Fe₂O₃) nanostructures and cephalexin antibiotic sorptive removal from polluted aqueous media. J Mol Liq. 2018;271:844-56. https://doi.org/10.1016/j.molliq.2018.09.057.

29. Cai J, Liu J, Gao Z, Navrotsky A, Suib SL. Synthesis and anion exchange of tunnel structure akaganeite. Chem Mater. 2001;13:4595-602. http://dx.doi.org/10.1021/cm010310w.

30. Gotić M, Dražić G, Musić S. Hydrothermal synthesis of α-Fe₂O₃ nanorings with the help of divalent metal cations, Mn²⁺, Cu²⁺, Zn²⁺ and Ni²⁺. J Mol Struct. 2011;993:167-76. http://dx.doi.org/10.1016/j.molstruc.2010.12.063.

31. Will G. Powder diffraction: the rietveld method and the two stage method to determine and refine crystal structures from powder diffraction data. Berlin: Springer; 2006. https://doi.org/10.1007/3-540-27986-5.

32. Fu X, Jia L, Wang A, Cao H, Ling Z, Liu C et al. Thermal stability of akaganeite and its desiccation process under conditions relevant to Mars. Icarus. 2020;336:113435. http://dx.doi.org/10.1016/j.icarus.2019.113435.

33. Parida KM. Studies on β-FeOOH. J Mater Sci. 1988;23:1201-5. http://dx.doi.org/10.1007/bf01154579.

34. Paterson E, Swaffield R, Clark DR. Thermal decomposition of synthetic akaganeite (β-FeOOH). Thermochim Acta. 1982;54:201-11. http://dx.doi.org/10.1016/0040-6031(82)85079-X.

35. Dézsi I, Keszthelyi L, Kulgawczuk D, McInár B, Eissa NA. Mössbauer study of β- and δ-FeOOH and their disintegration products. Phys Status Solidi. 1967;22:617-29. http://dx.doi.org/10.1002/pssb.19670220234.

36. Liu XQ, Tao SW, Shen YS. Preparation and characterization of nanocrystalline α-Fe₂O₃ by a sol-gel process. Sens Actuators B Chem. 1997;40:161-5. http://dx.doi.org/10.1016/S0925-4005(97)80256-0.

37. Musić S, Krehula S, Popović S. Thermal decomposition of β-FeOOH. Mater Lett. 2004;58:444-8. http://dx.doi.org/10.1016/S0167-577X(03)00522-6.

38. Shao HF, Qian XF, Yin J, Zhu ZK. Controlled morphology synthesis of β-FeOOH and the phase transition to Fe₂O₃. J Solid State Chem. 2005;178:3130-6. http://dx.doi.org/10.1016/j.jssc.2005.07.011.

39. Yang H, Bi Y, Wang M, Chen C, Xu Z, Chen K et al. β-FeOOH self-supporting electrode for eficient electrochemical anodic

oxidation process. Chemosphere. 2020;261:127674. https://doi.org/10.1016/j.chemosphere.2020.127674.

40. Li B, Yun Y, Wang M, Li C, Yang W, Li J et al. Superhydrophobic polymer membrane coated by mineralized β-FeOOH nanorods for direct contact membrane distillation. Desalination. 2021;500:114889. http://dx.doi.org/10.1016/j.desal.2020.114889.

41. Cho MK, Jo JH, Choi JU, Kim J, Yashiro H, Yuan S et al. Tunnel-type β-FeOOH cathode material for high rate sodium storage via a new conversion reaction. Nano Energy. 2017;41:687-96. http://dx.doi.org/10.1016/j.nanoen.2017.10.022.

42. Tang W, Zhang G, Qiu Y. FeOOH/Ni heterojunction nanoarrays on carbon cloth as a robust catalyst for efficient oxygen evolution reaction. Int J Hydrogen Energy. 2020;45:28566-75. http://dx.doi.org/10.1016/j.ijhydene.2020.07.022.

43. Li D, Xu R, Jia Y, Ning P, Li K. Controlled synthesis of α-Fe$_2$O$_3$ hollows from β-FeOOH rods. Chem Phys Lett. 2019;731:136623. http://dx.doi.org/10.1016/j.cplett.2019.136623.

44. Condon JB. Surface area and porosity determinations by physisorption: measurement, classical theories and quantum theory. 2nd ed. Amsterdam: Elsevier; 2019.

45. Groen J. Critical appraisal of mesopore characterization by adsorption analysis. Appl Catal A Gen. 2004;268:121-5. http://dx.doi.org/10.1016/j.apcata.2004.03.031.

46. Sing KSW. Reporting physisorption data for gas/solid systems with special reference to the determination of surface area and porosity (Recommendations 1984). Pure Appl Chem. 1985;57:603-19. http://dx.doi.org/10.1351/pac198557040603.

47. Katsuki H, Choi EK, Lee WJ, Hwang KT, Cho WS, Huang W et al. Ultrafast microwave-hydrothermal synthesis of hexagonal plates of hematite. Mater Chem Phys. 2018;205:210-6. http://dx.doi.org/10.1016/j.matchemphys.2017.10.078.

48. Villalba JC, Berezoski S, Cavicchiolli KA, Galvani V, Anaissi FJ. Structural refinement and morphology of synthetic akaganèite crystals, [β-FeO(OH)]. Mater Lett. 2013;104:17-20. http://dx.doi.org/10.1016/j.matlet.2013.04.004.

49. Malik V, Grobety B, Trappe V, Dietsch H, Schurtenberger P. A closer look at the synthesis and formation mechanism of hematite nanocubes. Colloids Surf A Physicochem Eng Asp. 2014;445:21-9. http://dx.doi.org/10.1016/j.colsurfa.2013.12.069.

50. Guo P, Wei Z, Wang B, Ding Y, Li H, Zhang G et al. Controlled synthesis, magnetic and sensing properties of hematite nanorods and microcapsules. Colloids Surf A Physicochem Eng Asp. 2011;380:234-40. http://dx.doi.org/10.1016/j.colsurfa.2011.02.026.

51. Liu L, Chen WT, Kihara S, Kilmartin PA. Green synthesis of akaganéite (β-FeOOH) nanocomposites as peroxidase-mimics and application for discoloration of methylene blue. J Environ Manage. 2021;296. http://dx.doi.org/10.1016/j.jenvman.2021.113163.